Modeling the Operation Regimes in Ultra-high Temperature Continuous Reactors

Sergiy S. Fedorov

February 2014

Nonproliferation and National Security Department

Brookhaven National Laboratory
P.O. Box 5000
Upton, New York 11973
www.bnl.gov

DISCLAIMER

This report was prepared as an account of work sponsored by an agency of the United States Government. Neither the United States Government nor any agency thereof, nor any of their employees, nor any of their contractors, subcontractors, or their employees, makes any warranty, express or implied, or assumes any legal liability or responsibility for the accuracy, completeness, or any third party's use or the results of such use of any information, apparatus, product, or process disclosed, or represents that its use would not infringe privately owned rights. Reference herein to any specific commercial product, process, or service by trade name, trademark, manufacturer, or otherwise, does not necessarily constitute or imply its endorsement, recommendation, or favoring by the United States Government or any agency thereof or its contractors or subcontractors. The views and opinions of authors expressed herein do not necessarily state or reflect those of the United States Government or any agency thereof.

Modeling the Operation Regimes in Ultra-high Temperature Continuous Reactors

Sergiy S. Fedorov[1], Mykhailo V. Gubynskyi[1], Igor V. Barsukov[2], Mykola V. Livitan[1], Brian S. Wells[2], Mayya Barsukov[2], Daria Zimina[2], Oleksiy G. Gogotsi[3], Yuliya Zozulya[3], Upendra Singh Rohatgi[4]

[1]National Metallurgical Academy of Ukraine, Dniepropetrovsk, Ukraine;
[2]American Energy Technologies Co., Arlington Heights, IL, USA;
[3]Materials Research Centre, Ltd., Kiev, Ukraine; [4]Brookhaven National Laboratory, Upton, NY, USA

1. Introduction.

In recent years the graphite and carbon industry has been rapidly evolving towards placing an ever growing emphasis on the production of ultra-high purity materials. The trend has been largely driven by downstream OEM customers whose applications increasingly call for the use of refined carbon materials in high-end products, which these companies sell on the consumer market.

One of such applications is the advanced battery market. The majority of batteries manufactured during the 1970-80s employed carbonaceous grades in their bill of materials which have the purity level on the order of 89 – 99wt%C[1,2],determined by the ASTM-referenced loss on ignition version of the test conducted at 815-950°C[3,4]. The surface detail of such materials can be traced to a Scanning Electron Microscopy image presented by Figure 1(a). The edge plane of graphite is peppered with trace mineral impurities. When inside a battery, these impurities may leach out from the surface of graphite, diffuse to the counter electrode and catalyze an undesirable evolution of gas. As our modeling shows, internal pressure buildup (Figure 1(b)) can lead to an eventual catastrophic rupture of a cell (Figure 1(c)).
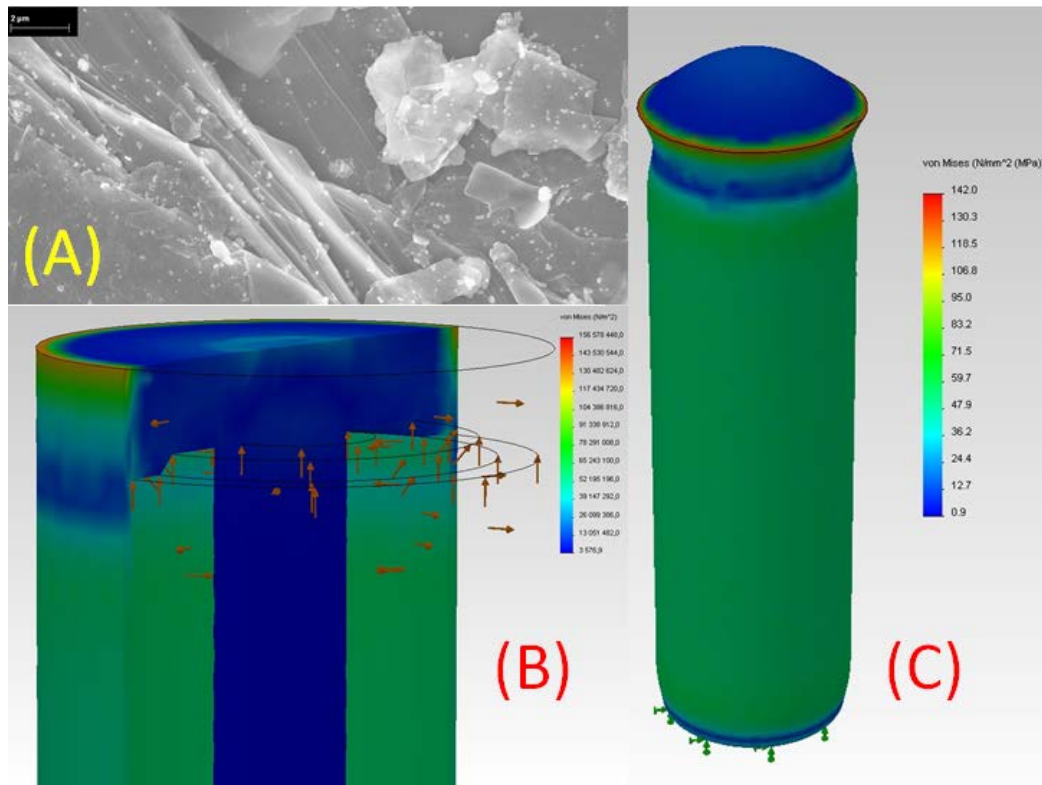

Figure 1. Sources and effects of gassing in batteries: *SEM of mineral impurities in graphite (a); modeling the effect of gas evolution inside an AA size cylindrical battery (static stress mapping): (b) a cutaway view of a stress model (deformation scale 1:1); (c) stress diagram of a cylindrical AA cell (deformation scale 104:1).*

Two decades ago the vast majority of aqueous battery systems relied heavily on the use of mercury and cadmium in their anodes. These heavy metals readily form protective amalgam on the surface of anode active materials, thus suppressing in-cell gassing. Due to environmental legislature prohibitions on land disposal of items containing cadmium and mercury, most consumer battery manufacturing platforms phased these additives out.[5] Alternative dopants to anodes were found and typically include Indium, Lead[5], and Bismuth.[6]

Primarily as a consequence of the industry transitioning to mercury-free batteries, some of the most stringent requirements to the purity levels of all battery materials, including carbons, were imposed. The battery industry has adopted the use of synthetic graphites[7,8], acid leached graphite[9,10] and thermally purified carbons[11,12]. Due to recognized environmental concerns associated with acid purification technologies[10], as well as the limited availability of feedstock and thermal balance inefficiencies in the production of synthetic graphite in Acheson furnaces,[13] a growing emphasis has been placed in recent years on the optimization of industrial thermal purification technologies for graphite and carbon[3,14].

One of the most efficient technologies for refining graphite and carbon is a continuous processing of graphitic raw material in electrothermal fluidized bed furnaces[15-25]. A typical reactor is shown in Figure 2. The presented furnace design allows for a continuous processing of granular carbon matter within the temperature range of 2,000 – 3,000°C. In doing so the following advantages of the process are ensured:

i. Uniformity of properties of the end product[25];
ii. Ultra-high purity of the resultant refined graphite[11];
iii. Precise control of degree of its graphitization[14, 26];
iv. Ability to operate on recycled sources of energy[25];
v. Continuous materials processing capability[24];
vi. Economic effectiveness[20];
vii. Flexibility of raw material selection, to include raw materials of natural, amorphous and synthetic origin, as well as recyclable carbon-containing wastes[23].

Under the auspices of projectBNL-T2-0372-UA by the US Department of Energy's National Nuclear Security Administration's Global Initiatives for Proliferation Prevention program, the authors conducted a systematic study into the hydraulic and thermal regimes of continuous electrothermal fluidized bed furnaces of our own design and manufacture.[18, 23, 24, 27, 28] Based on the vast experimental data collected in the course of hands-on furnacing campaigns, the authors have refined the legacy models whose purpose is to describe the processes which take place in the electrothermal fluidized bed specific to processing of industrial carbon and graphite. Some of these models proved to be useful for the industry in that they were used for engineering and scaled up manufacturing of large scale high temperature reactors and for selection of their operating regimes, irrespective of the furnace size and raw carbon material employed.

Figure 2. Cutaway view of a continuous electrothermal fluidized bed reactor:
1 – center electrode; 2 – lining of the overbed space; 3 - loading zone of graphite feed; 4 – active working zone of reactor; 5 – lower bed zone; 6 – cooling system (product exit); 7 – Feed bin.

2. Operating principle of the electrothermal furnace.

Please refer to Figure 2 as a description follows. The reactor operates around the clock in a non-stop, continuous regime. The interior of the furnace is made of two cylinders and a transitional conical piece which joins them. These cylinders are machined from graphite (2). The graphite inside the furnace is either a brick or a combination of brick and solid pieces, as appropriate. The interior volume of the active section of the reactor consists of three distinct zones. The upper section (2) is defined as an *overbed space*. The central section (4) is a *working area* or the *fluid bed zone*. The lower section (5) is the *lower*
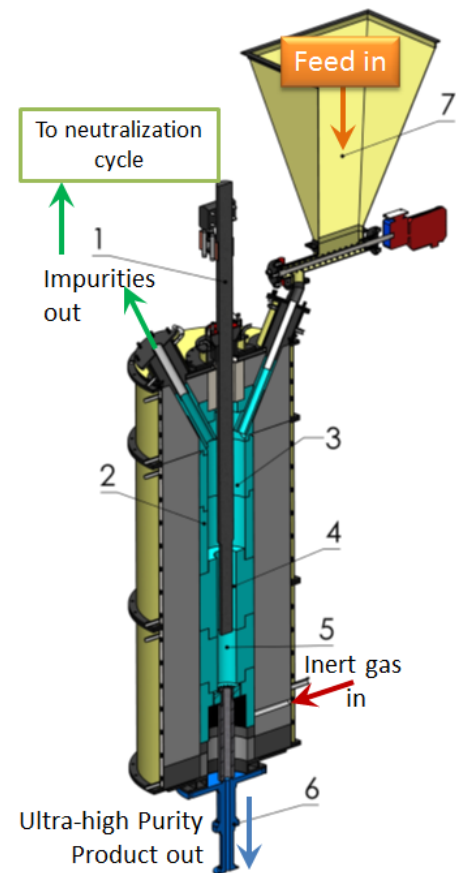
bed space. Hanging from the roof of the furnace is the central electrode (1) which is also made of graphite. When the furnace is operating, the lower segment of the center electrode is submerged into the fluid bed. A DC electrical current flows in a radial direction between the center electrode and the interior wall of the reactor. The current only flows when the furnace is filled with a critical concentration of electrically conductive particulates or granules. In a way, the fluidized bed resembles the electrolyte of a battery where the graphite particles which require thermal processing serve a similar function as ions in electrolyte.

The purpose of passing electrical current through the fluidized bed is to separate impurities from the graphitic core. With its sublimation point at 3,642°C in inert gas, graphite retains its stability in high temperature reactors operating on the principle of an electrothermal fluidized bed[30], while the actual working temperature on the order of 2,800°C is sufficient to decompose and volatilize virtually any impurity.

Fine mineral impurities are an integral part of conventional graphite. Their presence can be visually noted in the SEMs presented by Figure 1 (a) and 7 (b). They will readily evaporate from the surface of carbon particles assuming the temperature which is required for their decomposition and a sufficient dwell time in the hot zone is reached. The source of heating is a Joule heat - when the reactor is running, the graphite precursor particles are resistively heated by means of DC current while graphite is being gravity fed from the top of the furnace downward into the cooling zone.

The most active phase of heating graphitic feed occurs in the *working zone* where the distance between the electrode and wall is at a minimum. In order to increase the dwell time of particles in this area, a counter stream of inert gas (nitrogen) is introduced from the bottom of the furnace. The nitrogen ascends through the furnace flue and carries out subliming aerosols which are rich in volatilized foreign impurities. Graphite does not reach the flue and rather descends towards a discharge port in the bottom distributor plate. Slowing down its upward movement is a conical section in the reactor's inner wall which leads into a larger diameter chamber. Particles moving upwards readily lose their momentum and are effectively trapped in the overbed space. From this section, mostly sublimed aerosolizes which are loaded with mineral ash reach the flue zone. At later process stages these evaporated impurities undergo further combustion processing; traces which survive the latter get collected and neutralized to eventually form gypsum, while the ultra-pure graphitic product upon exiting the reactor undergoes further processing (i.e. grinding, sizing and surface treatment) to become battery-grade carbon.

3. Previous studies of mechanisms of electrothermal heat treatment of carbon in the fluidized bed.

Specific to the refining of graphitic carbons, electrothermal fluidized bed reactors were thoroughly investigated during the 1960-80s by scientific teams from the Institute of Heat and Mass Transfer of Belarus; The Gas Institute at the National Academy of Sciences in Kiev, Ukraine; McGill University, Montreal, Quebec, Canada; Iowa State University, Ames, IA, USA; Bethel Laboratories, Columbus, OH, USA and in a number of other organizations. Distinct contributions to the understanding of science and technology behind carbon material processing in fluidized bed reactors have been made by V.A. Borodulya, S.S. Zabrodskiy, A.I. Zheltov, Y.A. Buevich, A.P. Kozhan, B.I. Bondarenko, K.E. Makhorin, S.P. Gorislavets, W.M. Goldberger, P.R. Carney, M. Harrison, W. Krueger, M.S. Zak, P. Wikingsson, and other representatives of the international science, technology, engineering and business community.

As a consequence of hands-on experimental work performed and/or managed by these individuals, some of the most valuable data related to the dependence of specific electric resistance (SER) of graphite-filled fluid beds as a function of exterior processing parameters, yields, and lifetime was collected. The technology of refining graphite in fluid bed reactors has been fully commercialized in the former USSR, as well as in USA, Sweden and China.[31] Nevertheless there is still much to be understood and improved in the area of process technology, mechanisms, and physics of the fluid bed reactors. The development and modeling of new and improved high temperature reactors continues to be a highly sophisticated task. The authors therefore make an attempt to study carbon-rich fluid beds further.

4. The Specific Electric Resistance of the fluidized bed.

A task of designing high temperature reactors for refining graphitic carbon involves the determination of geometrical parameters of the working zone; to include the heights and diameters of reactor's main technological sections, as well as the diameter of the center electrode. In creating the model, a

synergistic consideration of hydrodynamic, electrothermal, chemical and thermal variables need to be considered.

The key characteristic for modelling is the Specific Electric Resistance (SER) of a fluidized bed. Its correct determination is paramount for engineering controls, as well as the reactor's geometry so as to achieve the targeted process temperature values and throughput rates. SER represents a complex function of the material type, particle size, current density, flue gas composition and a number of other process variables. Generally, SER reduces with the increase of current density, particle diameter, temperature, homogeneity and the height of the bed. The SER was seen to undergo an increase by a factor of 2 to 5 as a function of transition from dense to aggregating, or bubbling fluidization. The SER of a dense bed is 2 to 3 orders of magnitude greater than the SER of a stagnant material in a compressed form. Please refer to data in Table 1 which highlight these differences.

Table 1 – The Specific Electric Resistance of graphite as a function of its state.

State of graphite	SER, $\Omega \cdot$cm
Graphite electrode[32]	$8 \cdot 10^{-3}$
Dense bed consisting of graphite particles sized 0.07-1.2 mm[33]	5-10
Aggregating fluidized bed consisting of graphite particles sized 0.07-1.2 mm[33]	22-33

5. The mechanisms of electrical energy transfer.

The processes of resistive heating in a fluidized bed are complex in nature. Analysis of literature references[15,16,22,25], as well as our own experimental results suggest that the Joule heat is generated inside a reactor by at least two mechanisms. The first is due to multiple particle-to-particle collisions which induce electrical contact and in turn lead to resistive heating of graphite. The second is as a result of the appearance of short-lived lightning bolts which percolate the bulk of the bed when chains of particles contacting one another form spontaneous clusters which then contact neighboring clusters. In other words, constantly agitating particles collide to form electrically conducting chains; when their contact interrupts, electric micro-arcs may appear. There could be thousands of them at any given moment of time inside an operating reactor.

Another notable factor of fluid bed processing is the presence of gas channels and blisters inside the bed. The electrical conductivity of blisters is very low and must be considered as an important contributor to the overall electrical conductivity of the bed. Hollow channels are formed by nitrogen which ascends the working chamber in a counter flow to graphitic particulates. Gas channels are responsible for breaking up electrically conductive networks formed by graphite. The size and amount of gas bubbles in graphite matter significantly during processing.

These variables are taken into account in a dual phase model of fluidized bed.[34,35] This model assumes that the fluidized bed consists of two distinctly different phases: a quasi-dense graphite phase which resembles liquid emulsion and the
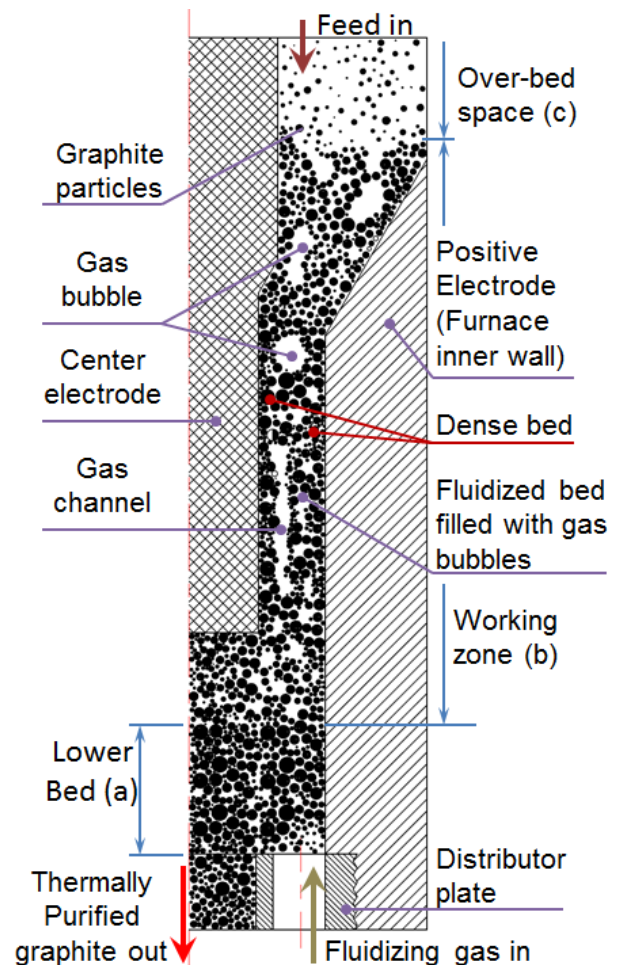

Figure 3. Segment cross section of a fluidized bed reactor for thermal purification of graphite.

fluidized gas-filled channels which are free of graphite but surrounded by the latter (Figure 3). Moreover, three areas of the reactor - the *working (active) zone (b)*; the *lower bed (a)*; and the *overbed space (c)* can be distinguished. These have different ratios of gas channels to graphite phase. Pore size distribution and size of channels are also different in each of these zones.

It is noteworthy that channels allow filtering massive amounts of gas through the bed. In the densest portion of the bed (section "b" in Figure 3), the throughput rate of fluidizing nitrogen is close to a critical threshold which defines the stability of a bed. A peculiar fact is that the dense phase of graphite moves predominantly down the walls formed by graphite lining and the central electrode; bubbles tend to concentrate predominantly in the center of the bed at some distance away from the limiting surfaces.

Analysis of equations (1) and (2) which define porosity of the bed in conditions of such a non-uniform fluidization indicates that the volume ratio of channels in graphite (density, $\rho = 2{,}050$ kg/m^3, effective particle diameter, $d_{particle} = 0.1$-1.0 mm) is small and possesses a value on the order of 5 vol %.

$$\varepsilon \ = \ \varepsilon_{mf} \cdot \left(\frac{Re + 0.02 \cdot Re^2}{Re_{mf} + 0.02 \cdot Re_{mf}^2} \right)^{0,1} ; \qquad (1)$$

$$\varepsilon \ = \ \delta + (1 - \delta) \cdot \varepsilon_{mf}, \qquad (2)$$

Where ε is the porosity of a non-uniform fluidized bed; $\varepsilon_{mf} = 0.4$-0.45 is the critical porosity of the fluid bed on the border line of maximum achievable stability of the bed; Re and Re_{mf} are the Reynolds numbers (dimensionless values which characterize the ratio of nonlinear and dissipative terms in the Navier - Stokes equations) for the fluidized bed and dense bed when it is at the threshold of losing its stability; δ - is the volume ratio of gas channels.

As the results of our modeling indicate (Table 2), in the above conditions, gas channels reduce the effective surface area of the fluid bed but their influence is not significant.

Table 2 - Influence of the volume fraction of channels on the
Specific Electrical Resistance of the bed (results of numerical modeling).

Volume fraction of channels δ, %	1	3	5	7
Increase of SER of the fluid bed over that for a dense bed, %	2.4	5.3	8.3	11.6

6. Structure of the fluidized bed and its influence on the value of Specific Electrical Resistance.

As one can see from the schematic presented in Figure 3, the fluid bed consists of three main zones. The first segment (a) is located just above the distributor plate. It is known as the *lower bed space*. This zone is only few centimeters tall, but is where blisters of gas initially form. The working zone of the fluid bed (b) represents the main segment of a process reactor. This is where blisters of gas grow in size, rise and combine to form straight through channels (an undesirable phenomenon which must be avoided).[35] There is also the over-bed zone (c) where bubbles which come to the surface burst, and where the bed gains both returning and fresh carbon particles.

In the lower bed zone, the fluidized bed is characterized by high porosity. It is typical to see high homogeneity of graphite particle distribution in this part of reactor. Consequently, local electrical resistance in this zone is significantly higher than the average resistance for the entire height of the bed. Borodulya *et al.* have experimentally confirmed this to be true.[36]

In the over-bed space, clusters of particulates which have burst from the main zone are fluffed, mostly disaggregated and free-flowing; consequentially this section's porosity increases to near 100% and as a result the electrical current is almost nonexistent.

The only area of the bed which significantly impacts the value of electrical resistance is the active working zone (b). This is where the most active phase of channel development takes place. For the given graphite precursor, the regime of forming gas channels corresponds to the fluidization criteria *W*, which falls on the range of 1<*W*<2. It should be noted that at an increased gas velocity the system goes into a pulsing fluidization regime which results in a height reduction of the blister zone; the taller this area, the more dramatic the increase of SER. It should be noted that pulsing channels format a height which corresponds to a ratio of H/D>1 (H is the height from the distributor plate to the imaginary line where the gas channels begin to form and D is the effective diameter of a distributor plate).

7. The effect of electric contact between particles.

As it has been mentioned earlier, the working zone of a fluidized bed reactor is filled with non-homogeneous electrically conductive networks of graphitic particles. These form spontaneously as individual particles of graphite collide. The network resistivity is defined by the contact surface area of two individual granules. It makes sense to define the above area as a "footprint" of contact between two particles; the radius of such footprint is assumed to be known and equal to *a*. This parameter is a function of a value of compressive pressure between two particles, P; and the number of surfaces in a particle which are available for contact, N. It should be understood that in fluid bed reactors particle-to-particle contact is highly unreliable and short lived. Application of pressure between particles is ensured by pulsation of the bed. Considering instability of the above parameters, the electrical resistance of the active layer is a dynamically alternating variable. The frequency of SER changes is a reflection of the pulsation frequency of the entire system. Our experimental results suggest that this frequency ranges from 2 to 7 Hz – a range which we have observed on the cold model described earlier[24] (please see Figure 4).
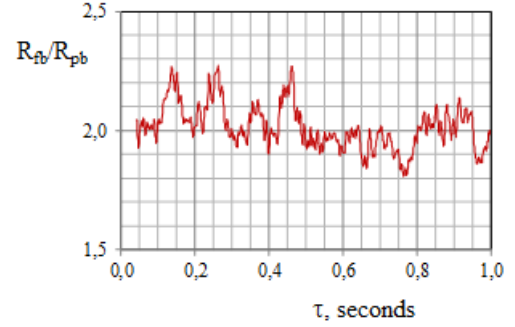

Figure 4. Oscillogram of the relative resistance of fluidized bed of graphite GT-1, Zavalye Graphite, Ltd. (ρ = 2,050 kg/m^3, effective particle diameter, $d_{particle}$ = = 0.25 mm; fluidizing agent – air, t = 50°C, W = 2; R_{fb} – electrical resistance of the fluid bed, Ω; R_{pb} – electrical resistance of the stagnant bed of graphite, Ω).

The coordinate number for the fluid bed N can be estimated from the equation (3):

$$N = \frac{\varepsilon_{mf} + 3 + \sqrt{\varepsilon_{mf}^2 - 10 \cdot \varepsilon_{mf} + 9}}{2 \cdot \varepsilon_{mf}}. \tag{3}$$

When the value of ε_{mf} = 0.4-0.45, N falls in the range of 6.2 – 7.1 for an operating fully loaded fluid bed. Near the wall (i.e. the graphitic lining of the reactor and the central electrode) the porosity of the bed is on the order of 0.6 (60%) and the number of particle-to-particle contacts is estimated at approximately 4.4. The porosity within the working zone of the bed and the number of particle-to-particle contacts differs insignificantly along its height. Therefore, the predominant influence on SER comes from particle compression pressure, P. Noteworthy, electrical resistance of the zone which lay adjacent to the wall is somewhat higher at the account of lower compaction density of the moving particles in this portion of the bed. We stipulate that the influence of the wall effect on the overall SER of the reactor is in reverse proportion to the diameter of the reactor.

The author[38] conducted an analysis of granular structure which has an overall cubic shape (N=6), and is formed of spheroidal particles. He has shown that SER does not depend on the number of contacts between individual particles. This conclusion was based on an assumption that a cubic interconnected shape is filled with serial and parallel particle-to-particle chains whose individual SERs cancel out. Consequentially, the SER of such a fluid bed can be described by the equation (4):

$$\Omega = \Omega_0 \cdot \frac{d_{particle}}{a} \tag{4}$$

In the above equation Ω is the SER of a fluidized bed layer, $\Omega \cdot$cm; Ω_0 is the SER of a material being processed; $d_{particle}$ the effective average diameter of particles, mm; *a* - the radius of a particle-to-particle contact imprint. The author of this work proposes to work with *a* = 8 μm.[38] However, the question remains open as to the applicability of the above value for packing arrangements which are not cubical. Moreover the model proposed by equation (4) does not factor in the influence of pressure, surface properties of granules, and their resiliency (e.g. spring back of material in response to the applied pressure).

A more sophisticated physical model describes the electrical conductivity of granular matter as a complex function of particle size, number of particle-to-particle contacts, applied stress and surface roughness.[37] The authors propose to base the solution on the calculation of elastic deformation which appears upon contact interaction between two spherical bodies (the Hertz problem). The latter has to be

adjusted to include structural peculiarities (i.e. surface roughness) of granular shapes. Using this approach, the following equations were derived for the electrical conductivity of the dense segment of a fluid bed, Λ:

$$\Lambda = \frac{G}{G_0} = \left(\frac{y_1}{y_4}\right)^2 \cdot \left(0.5\cdot\overline{h_{sh}} + \left(1-0.5\cdot\overline{h_{sh}}\right)\cdot\Phi\right)^{-1} \tag{5}$$

$$y_4 = \frac{2\cdot\sqrt{N-1}/N}{\sqrt[3]{1-\varepsilon}} \tag{6}$$

$$\Phi \approx 0.017 + 0.4\cdot y_1 \tag{7}$$

$$\overline{h_{sh}} = \frac{h_{sh}}{d_{par}/2} \tag{8}$$

$$y_1 = K\cdot\sqrt{\eta}\cdot\sqrt[3]{(1-\varepsilon)^{-2/3}\cdot P} \tag{9}$$

In the above equations $G = \Omega^{-1}$ is the specific electrical conductivity of material, S/m; $G_0 = \Omega^{-1}$ is the specific electrical conductivity of the fluid bed, S/m; y_1 is the actual estimated average radius of the contact footprint between two particles (the value has to factor in surface roughness); h_{sh} is the surface roughness of material, mm; P is the load applied to the fluid bed, Pa; $K= 3,3\cdot10^{-3}$ is a coefficient which factors in an estimated resiliency of granular structure; $\eta = (0.001 \div 1)\cdot10^{-2}$ is the relative estimated area of actual contact between the particles (depends on form factor, size of the micro roughness, strength modules and the value of external pressure).

P. Kozhan et $al.$[33]developed comprehensive experimental data for the values of electrical resistivity of graphite-filled fluid bed reactors with the goal in mind to accurately estimate the contact footprint y_1 and the surface roughness h_{sh} variables which are part of equation (5). The values of surface roughness which were estimated as part of numerical modeling were: $h_{sh} = 1.5\cdot10^{-3}$ mm and the particle-to-particle contact footprint $y_1= 2.5\cdot10^{-3}$. These correlate well with Kozhan's experimental data as summarized in Tables 3 and 4. Noteworthy, the value of SER for graphite was estimated using the equation (10):[32]

$$\Omega_0 = \left(1.37 + 1.1\cdot e^{(1,273-T)/564}\right)\cdot10^{-3}, \Omega\cdot cm, \tag{10}$$

Where T is the estimated average temperature of the fluid bed, K.

**Table 3 – Influence of graphite particle size on
the Specific Electrical Resistance of fluid bed (Temperature: 20°C).**

Particle diameter, mm	SER, $\Omega\cdot cm$	
	Modeling per (5-10)	Experiment[33]
0.105	34	33
0.195	27	27
0.375	23	24
0.850	21	23

Given the accuracy established above, equations (5) through (10) were regarded to be suitable for modeling of graphite heat treatment processes in the fluid bed reactors. They were used as a foundation of modeling and engineering work which has since unfolded within our team. These functions have proven useful for design of a pilot furnace with a throughput of 10 kg/hour (Figure 5).

Table 4 – Influence of Temperature of fluidized bed on the Specific Electrical Resistance.

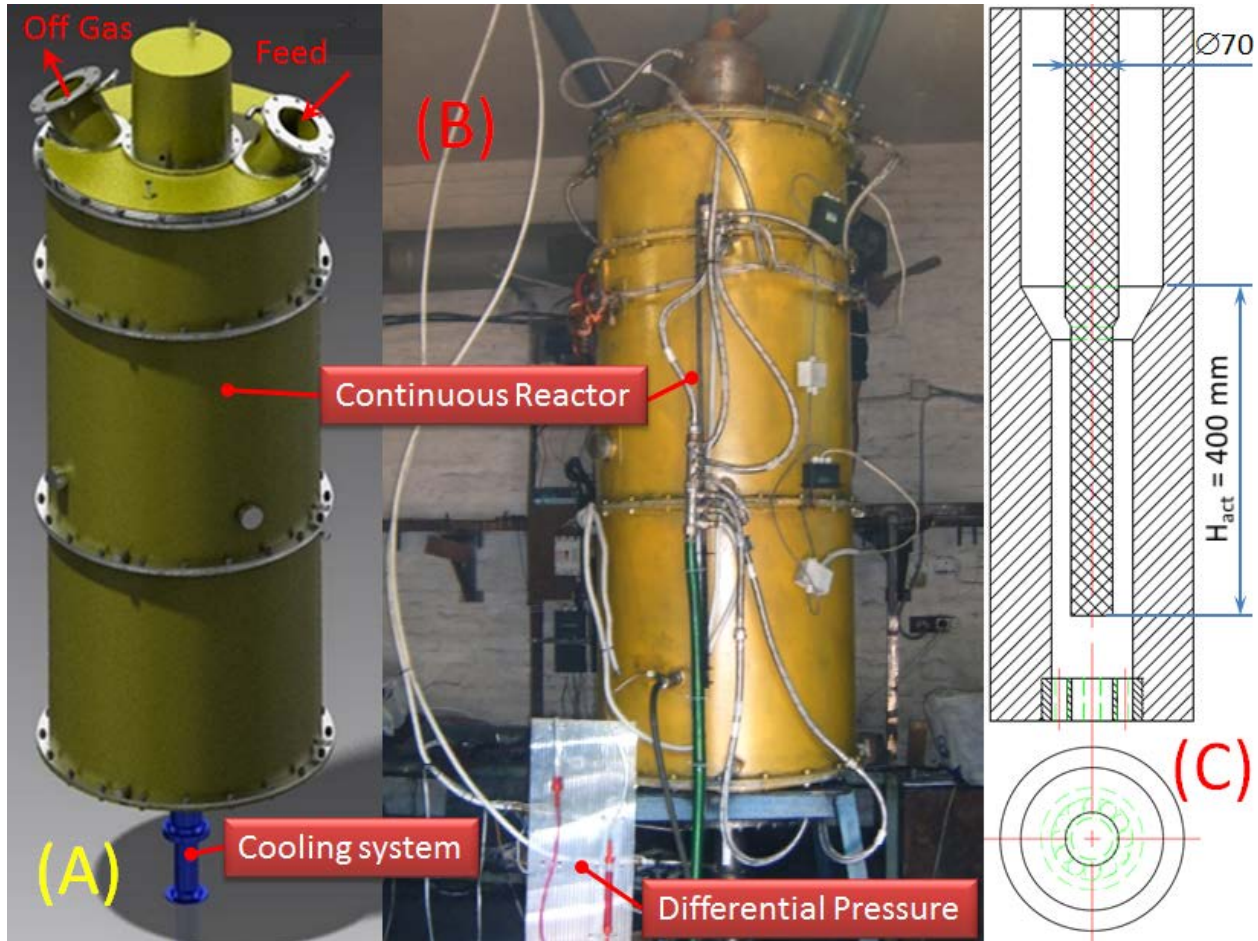| Fluid Bed Temperature, °C	SER, $\Omega \cdot$cm	
	Modeling per (5-10)	Experiment[33]
200	18.0	17.0
500	12.3	10.8
800	9.0	8.5

Figure 5. Pilot Continuous Electrothermal Fluidized bed reactor:
(a) Engineering model; (b) actual reactor; (c) schematic of the active fluidization zone.

Please refer to Figure 5 which represents schematics and the actual continuous high temperature pilot reactor which has been built as part of US DOE project BNL-T2-0372-UA. The inner diameter of the active zone of the furnace is D_{act} = 105 mm; the height of an active zone is H_{act} = 400 mm. The diameter of the center electrode is D_2 = 70 mm (Figure 5 (c)). For the purpose of added flexibility in operating the furnace, along the electrode length of 250 mm from the bottom, the latter has been reduced in size on a lathe to the diameter D_1 = 50 mm.

The average SER value for the given design was calculated per equation (11):

$$\Omega = \frac{2 \cdot \pi \cdot U^2}{W} \cdot \left(\frac{H_1}{\ln \frac{D_{act}}{D_1}} + \frac{H_2}{\ln \frac{D_{act}}{D_2}} \right) \cdot 10^2, \ \Omega \cdot \text{cm} \tag{11}$$

8

In the above formula, U is operating voltage, V; W is the power consumption of reactor, W; $H_1 = 250$ mm is the portion of the height of active fluid bed zone which is covered by the diameter of center electrode $D_1 = 50$ mm; $H_2 = 150$ mm is the portion of the height of active fluid bed zone which is covered by the diameter of center electrode $D_2 = 70$ mm.

The raw material used in the experiment is natural crystalline flake graphite GT-1 by Zavalyevskiy Graphite Ltd., Kyiv, Ukraine.[39] Its purity is LOI = 92 wt% C; Ash = 7 wt%; Volatiles (including moisture): 1 wt%. Sieve particle size distribution for the grade used is presented in Table 5. Overall the fraction studied falls within a range 0.025 – 1.0 mm; the average particle diameter is 0.25 mm.

Table 5 – Sieve analysis data for graphite GT-1.

Sieve opening, mm	1	0.5	0.4	0.3	0.2	0.1	0.05	0.025
Weight Percent in a Distribution, %	0.01	0.125	1.76	35.8	53.2	7.57	0.98	0.555

The SER of the graphite was determined experimentally per.[40] In accordance with the method, a specific size fraction and volume of sample is confined under load in a non-conductive cylindrical mold by two metal electrodes. Unidirectional resistance is measured between these electrodes using a Kelvin bridge. Resistivity is calculated and reported in $\Omega \cdot$cm. It measured 7.1-$9.8 \cdot 10^{-3} \Omega \cdot$cm which agrees with (10). Testing of the furnace presented in Figure 5 (a-b) was done in a full working regime, with current supplied into the bed while graphite GT-1 was loaded into the furnace. The temperature inside the furnace was measured indirectly with the help of two thermocouples planted into the outer lining of the furnace 70 mm inside the outer metal shell of the reactor. The first thermocouple read temperatures on the center level of the active zone, while the second was placed near the furnace flue (both can be seen in Figure 5 (b)). The temperature of heat treated graphite product after unloading from the cooler system (Figure 5 (a)) was performed by the direct contact method. During the heat-up of the furnace the following parameters of the process were input over these ranges:

    i.   Power: 4 – 8.5 kW;
    ii.   Voltage: 6 – 17 VDC;
    iii.   Current: 400 – 650 A;
    iv.   Inlet pressure of fluidizing gas (Nitrogen): 260 – 400 mm H_2O;
    v.   Nitrogen throughput: 8 – 26 Liters / min.

Using the above process parameters we were able to achieve the temperature of graphite on the order of 800°C. The results of this start-up run calculated vs. actual are summarized in Table 6.

Table 6 – Results of the Experimental run.

Property	Beginning of the Heat up	The end of the Heat up
Voltage, U, V	16.3	6.3
Current, I, A	430	637
Electric Power, kW	4,6	4.0
The Temperature of Material, °C	20	700-800
SER of the fluid bed, $\Omega \cdot$cm	17.0	8.39
SER of the fluid bed per numerical model (5 - 10), $\Omega \cdot$cm	25.30	10.24

Some of the published data of experimental studies in the electrothermal fluidized bed reactors[15,16] points out that the reduction of SER takes place with an increase of the current density supplied into the bed. The physics of such phenomena are not completely understood. The author[16] links these phenomena to the change of a mechanism of electrical conductivity within the fluidized bed from pure particle-to-particle contact to contact-ionizing mechanism. Assuming there is room for ionization of gas inside the fluidized bed reactors at the ultra-high temperatures, as well as recognizing the fact that

equation (5) may need to be adjusted for processes which are accomplished in the temperature range of 2,000-2,800°C (i.e. thermal purification of graphite for advanced batteries), we applied a regression relationship for SER to the experimental data[16] on process temperature and current density (12):

$$\Omega = 0.01 \cdot (84.711 - 2.593 \cdot 10^{-2} \cdot t - 46.854 \cdot i + 1.205 \cdot 10^{-2} \cdot t \cdot i), \Omega \cdot m. \tag{12}$$

This relationship is believed to be accurate for graphitic carbons ($d_{particle}$ = 0.130 mm) in the temperature range t = 0 – 2,800°C and current density i = 0.004 – 1 A/cm^2. The equation is valid under the assumption that an unrestricted aggregating fluidization in its classic form is taking place in a reactor.

8. On the numerical methodology of developing electrothermal fluidized bed reactors.

In developing high temperature reactors of the fluid bed type, one has to consider a complex task where geometrical parameters of the reactor are tied in with the properties of available power supply, and simultaneously tailored for the properties of material being processed. Overall, the sequence of designing the industrial fluidized bed reactors consists of the following steps:

1. Select working geometry of the furnace taking into account the desired furnace throughput, specific types and properties of available raw materials, hydrodynamics of the fluidized bed as a function of dwell time and process temperature;
2. Engineering of the external geometry of the furnace to include the thickness of thermal insulation;
3. Determine energy efficiency properties of the reactor (perform material and heat balance calculations);
4. Calculate main aspects of technology to include current, voltage, throughput of material and that of the fluidizing gas. At this stage the power supply for the furnace is selected.
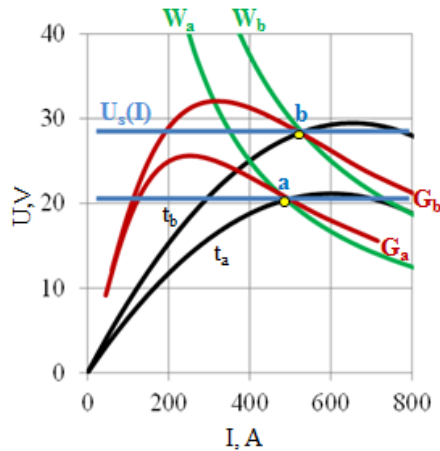

Figure 6. Numerically modelled properties of Electrothermal Fluid Bed Reactors: *a and b – working areas for selected operations regimes; t – Voltamogram of the fluid bed for a given temperature (t_b<t_a); G – Voltamogram of the furnace at the given throughput (G_b>G_a); W – parallel lines of constant voltage (W_b>W_a); $U_s(I)$ – Voltamograms of the power supply.*

Refining answers to the above questions over several iterations ultimately leads to optimization of the reactor design as well as regimes of its operation. Few specific examples follow.

When it comes to selection of processes of heating regimes for the reactor, we have developed an iterative algorithm which is based on the analysis of Voltamograms of the electrothermal fluidized bed, the furnace, and the power supply. All three have to be considered simultaneously in conjunction with each other as introduced in Figure 6.

The Voltamograms of the electrothermal fluidized bed at the given temperature (t=constant) is represented by solid black lines in Figure 6. These lines are plotted from the data feeds generated from equations (13) and (14):

$$U = \frac{I}{R}; \tag{13}$$

$$R = \frac{\Omega \cdot \ln \frac{D_{lining}}{D_{electrode}}}{2 \cdot \pi \cdot H_{active\ zone}} \tag{14}$$

Where D_{lining} is the diameter of the active zone of the furnace; $D_{electrode}$ is the diameter of the center electrode in meters; $H_{active\ zone}$ is the height of the working zone of the reactor, m; Ω is the SER of a fluidized bed which has been derived in (12).

The Voltamograms of the furnace at the constant throughput rate (G=constant) are outlined by red curves. Values of working current and voltage are selected from the energy input required. The latter are calculated from the heat balance of the reactor for varying temperatures of heat treatment, and factoring in the values of electrical resistivity of fluid bed, as calculated from (12):

$$I = \sqrt{\frac{W}{R}};$$ (15)

$$U = \sqrt{WR}.$$ (16)

In the above expressions, $W = Q_{fp} + Q_{N2} + Q_d + Q_v + Q_{H2O} + Q_{cool}$, where Q_{fp} is the actual heat value of the finished product; Q_{N2} is the physical heat value of nitrogen; Q_d is the heat value of dust exiting the furnace; Q_v is the actual heat value of volatile matter (organics and moisture); Q_{H2O} is the heat value of vapor (considering the loss resulting through the aerosol phase) and Q_{cool} is the heat loss due to external cooling.

Due to the fact that SER calculated per formula (12) is a function of current density, one needs to solve equation (15) using an iterative numerical approach.

Green curves in Figure 6 refer to voltamograms of power input of the furnace, W. A condition W = constant is typically assumed in operating reactors. Using graphs in Figure 6 and also equation (17) one can determine parameter W and derive Voltage, U and current, I from the latter:

$$U = \frac{W}{I}.$$ (17)

The voltamograms of power supply are shown in Figure 6 by blue lines. In this particular example we show a non-flexible power supply whose $U_s(I)$ = constant. It should be understood that there is a great variety of power supplies on the market and in some the voltage may not be a fixed line. Overall, the area of the graph presented by Figure 6, where red and black curves intersect (points *a* and *b*), should be regarded as characteristic points which define the relationship between the voltage and current which are required in order to achieve the desired process temperature and throughput rate, given the chosen reactor geometry (i.e. diameter of center electrode, the height and diameter of working zone and given thickness of thermal insulation). Correspondingly, the voltamogram of power supply has to correspond to the working regimes defined by points *a* and *b* on the graph.

Proposed methodology has been used in the development and construction of a fully functional continuous electrothermal fluid bed reactor with the throughput of 10 kg/hour (Figure 5 (b)). Numerical calculation of furnace parameters specific to thermal purification of flake graphite GT-1 at the temperature of 2,000°C required the following engineering inputs: I = 600 A, U = 27 VDC; $H_{\text{working zone}}$ = 350 mm; D_{lining} = 105 mm, $D_{\text{electrode}}$ = 60 mm.
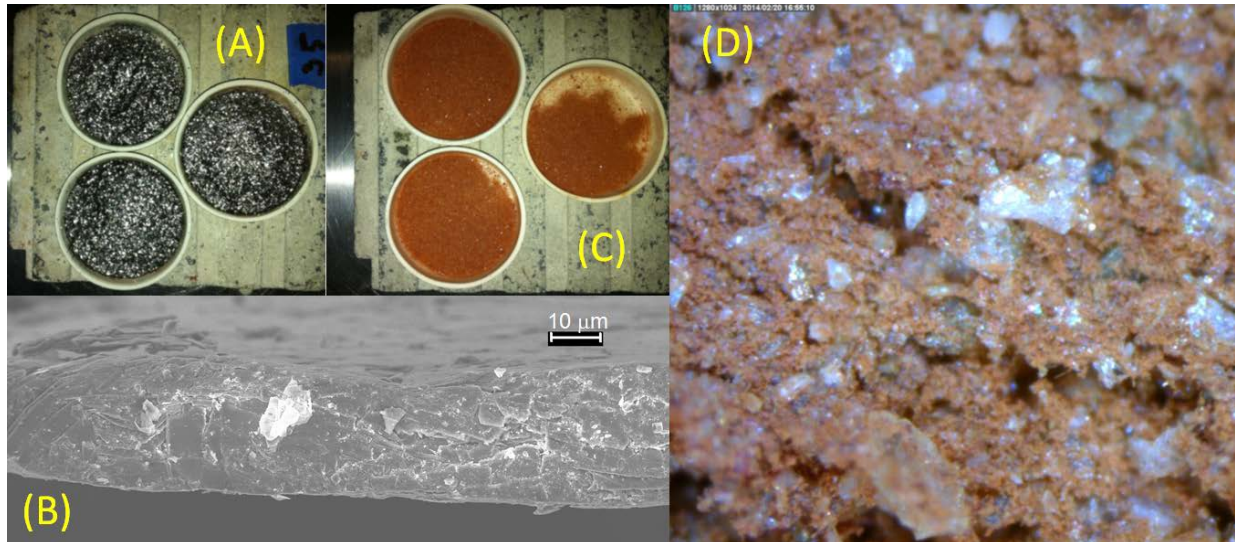

Figure 7. Ash analysis in the precursor graphite (prior to thermal purification):
(a) Coors ceramic crucibles which hold 1.0000 +/- 0.0001 g of precursor graphite each; (b) SEM of the edge plane of precursor graphite prior to ashing; (c) ash residue of samples depicted in (a) after LOI test; (d) Optical microscopy image of the ash residue from the samples depicted in (c), magnification x500.

9. Experimental methodology for qualifying the effectiveness of natural crystalline flake graphite purification in the fluidized bed reactors.

There are multiple analytical methods which the industrial carbon industries use to qualify how well the refining furnaces purify graphite precursor. In this paper we describe an ASTM-referenced variation of the loss on ignition test (LOI)[41] which authors believe to be fully adequate for accurate express control of the effectiveness of thermal purification in the fluidized bed reactors.

In accordance with this method, a desiccated low-profile ceramic crucible which has been precooked at 950°C and cooled down to room temperature prior to the test is loaded with 1.0000 +/- 0.0001 grams of graphite (Figure 7 (a)) and placed into a muffle furnace. The graphite powder is allowed to oxidize at a temperature of 950 +/- 5°C to a constant weight (in the case of this experiment a 4-hour dwell time proved to be sufficient). The residue (Figure 7 (c)) corresponds to the amount ash content. Its weight is expressed as percentage of the initial sample weight.

Figure 8. Schematic representation of impurities in graphite: *1 – graphite basal plane; 2 – mineral ash; 3 – moisture (volatiles).*

As introduced by modeling presented in Figure 1, ash in carbon may be a significant problem when used in advanced battery systems. In order to develop a better level of understanding as to where the ash is located in graphite and how it looks, we analyzed individual flakes which are depicted in Figure 7 (a) using Scanning Electron Microscopy (SEM) method. We used a Zeiss Supra 50 VP (resolution 1.3 nm) state-of-the-art field-emission SEM equipped with EDS and WDS detectors. The appearance of a precursor flake graphite particleatx836 magnification at 7.0 kV is shown by Figure 7 (b).

In analyzing Figure 7 (b) one may clearly see that 200+ micron flake graphite particles are peppered with mineral impurities which are typically 1 to 10 μm in size. An optical image of ash residue recovered from a 4 wt% non-combusted fraction shown in Figure 7 (c) reveals presence of a multi-colored bed of impurities (Figure 7 (d)). The brown and red colors reflect iron-rich pyrite residue; clear white and tan rocks reveal presence of calcites, silicates and marble rock. Noteworthy these impurities are not just sitting on the surface; they are also folded into the flake and sometimes percolate the basal plane. The precursor graphite also has residual moisture in its composition which could be as high as 0.1 wt%. The overall schematic representation of impurities in graphite is given by Figure 8.

Thermal purification in the continuous fluidized bed reactors which are described in this paper is precisely aimed at getting rid of the above impurities.

Please refer to Figure 9 which depicts the LOI test results with graphite from Figure 7 (a) which has been thermally purified in a continuous pilot fluidized bed furnace at 2,400°C.
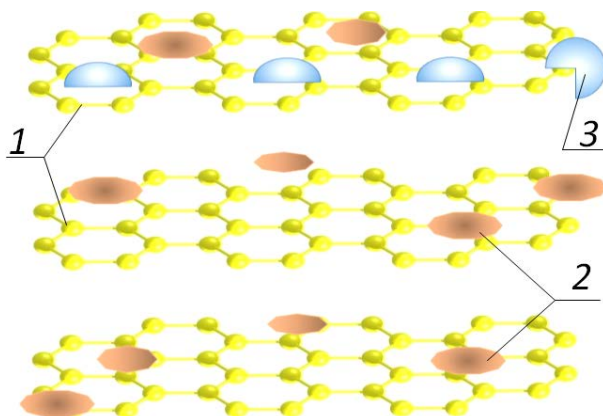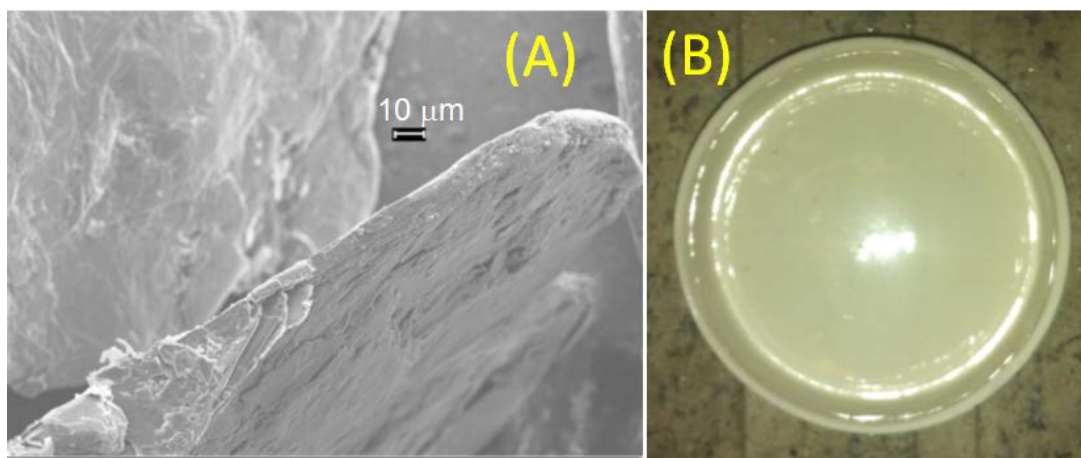
Figure 9. Results of thermal purification of graphite in a continuous electrothermal fluidized bed reactor: *(a) SEM of refined flake; (b) ash residue from the above after the LOI test.*

Analysis of the data presented in Figure 9 (b) reveals that there is hardly any ash left in the graphite structure after it has undergone a refining process in a fluidized bed reactor at temperature of 2,400°C. Specifically, ash amounted to 0.01 wt% of the starting sample which corresponds to graphite purity of 99.99%C – a suitable level of purity for advanced battery applications.

Independent verification of the effective purification can be seen in Figure 9 (a). The SEM of the edge plane of the resultant graphite particle recorded at magnification x502 at 7 kV reveals a clean surface of graphite which is essentially free of foreign impurities.

10. Conclusions.

High temperature refining in continuous electrothermal fluidized bed reactors unveiled in this paper reliably produce graphite whose high purity of 99.99%C sets the industry standard for applications in advanced battery systems. This technology is environmentally benign, economically viable and, when fully scaled up to the industrial volume, will present a viable alternative to acid leached natural crystalline flake graphite and synthetic graphite produced in batch Acheson reactors.

One of the most critical parameters of an operating fluid bed is the value of specific electrical resistance (SER) of the bed. Authors proposed a numerical model and unveiled a methodology for estimating the value of SER specific to fluidized bed reactors for purification of natural flake graphite. The model which is believed to be accurately describing processes in fluidized bed reactors is believed to be a dual phase one where an emulsified dense graphite bed moves along the limiting surfaces formed by the center electrode and reactor lining, and a gas-channels-filled aggregating bed forms at some distance away from the solid graphite walls toward the middle of the bed.

Application of the above model was verified in the course of hands-on experiment. The model was determined to be accurate with a maximum 25% deviation from actual test data, which is a great result considering that processes of fluidized beds are complex systems.

Using this model authors have derived a regression expression which allows to estimate values of SER for particles of flake graphite in a temperature range from 0 to 2,800C, and for the current density i = 0.004-1.0 A/cm^2. From there a methodology for designing fluidized bed reactors for purification of carbon has been proposed. This methodology allows to define the geometry, key dimensions, current, voltage, power, as well as to specify properties of the power supply for the reactor; given the designer knows a desired furnace throughput rate, operating temperature and material dwell time in the hot zone. The basis for the reactor design is the creation of voltamograms for the bed, furnace, and power supply, and plotting them on the same graph so as to identify overlapping areas.

Based on the above models, a fully functional prototype reactor whose throughput rate is rated at 10 kg/hour has been engineered, built, and tested. Thermally purified material was analyzed using the loss on ignition test and by the Scanning and Optical microscopy methods.

Literature.
1. Grades of graphite and specifications: Product GE-3. Zavalyevskiy Graphite Ltd., Kyiv, Ukraine (2012).
2. Signature Graphite and Carbon: Products 9800, 2590. Superior Graphite Co., Chicago, IL, USA (1998).

3. I. Barsukov, M. Gallego and J. Doninger. Novel materials for electrochemical power sources – Introduction of PUREBLACK® Carbons. J. Power Sources 153 P. 288-299 (2006).

4. Analytical procedures for TIMREX® Graphite and Coke. In *A Synopsis of Analytical Procedures*. Timcal, Ltd. Group, Bodio, Switzerland P. 4 (2008).

5. Handbook of Batteries. / D. Linden, T.B. Reddy.- 3rd ed. McGraw Hill, New York, NY, P.35.1 (2001).

6. H.W. Sarkas and I.V. Barsukov. Zinc Anode Alkaline Electrochemical Cells Containing Bismuth. US Patent Appl. Docket No. NTC02-032-US (2013).

7. M.E. Spahr. Carbon Conductive Additives for Lithium-Ion Batteries. In Lithium-Ion Batteries (M. Yoshio, R.J. Brodd and A. Kozawa eds.), Springer Science+Business Media, LLC, New York, NY, P. 117 (2009).

8. G. Juri, H. A. Wilhelm and J. L'Heureux. High-Purity Graphite Powders for High Performance. Timcal, Ltd. Group, Bodio, Switzerland (2010).

9. Y.F. Lia, S.F. Zhu, L. Wang. Purification of natural graphite by microwave assisted acid leaching. Carbon. V. 55 (4) 377–378 (2013).

10. H. Lazenby. Northern Graphite develops proprietary purification technology. Mining Weekly International. The Creamer Media Publ. 30/9/2013, Bedfordview, Johannesburg, South Africa (2013).

11. I.V. Barsukov, J.E. Doninger, P. Zaleski and D. Derwin. Recent developments on the use of graphite in alkaline battery systems. ITE Letters on Batteries, New Technologies and Medicine, v. 2, 1, P. 106-110 (2000).

12. F-X Henry, I.V. Barsukov et al. New Developments in the Advanced Graphite for Lithium-ion Batteries. I.V. Barsukov et al (eds.), New Carbon Based Materials for Electrochemical Energy Storage Systems: Batteries, Supercapacitors and Fuel Cells. Springer P. 213-229 (2006).

13. A.V. Tamashausky. An Introduction to Synthetic Graphite. Asbury Graphite Mills Inc. Asbury, NJ, USA Publ. P. 12 (2006).

14. P. Booth, J.E Doninger, I.V. Barsukov, M.S. Zak, R.L. Taylor, J.A. Ayala, D. Tandon. Thermally modified carbon blacks for various type applications and a process for producing same. US Patent Application 20050063892-A1 (2003).

15. C.K. Gupta, D. Sathiyamoorthy. Fluid bed technology in materials processing. CRC Press. Boca Raton, FL, USA. 528 (1999).

16. V.A. Borodulia. High-temperature processes in electrothermal fluidized bed. Nauka i Technika Publ. House. Minsk, USSR 173 (1973) – in Russian.

17. M.V. Gubynskyi, S.S. Fedorov, M.V. Livitan, O.G. Gogotsi, I.V. Barsukov, and U. Rohatgi Analysis of energy efficiency of furnaces for high-temperature heat treatment of carbonaceous materials. J. Metallurgical and Mining Industry, N2. 88-91 (2013) – in Russian.

18. M.V. Gubynskyi, S.S. Fedorov, M.V. Livitan, I.V. Barsukov, O.G. Gogotsi, N.P. Brodnikovskiy. Furnaces for manufacture of high purity carbonaceous materials. In the book of Proc. of Conference: "Theory and Applications of Heat Processes in Metallurgy." 18-21/9/2012, URFU Publ., Yekateringburg, Russia, p. 79-83 (2012) – in Russian.

19. M.S. Zak, W.M. Harrison, J.E. Doninger. Method and Apparatus for Heat Treatment of Particulates in an Electrothermal Fluidized Bed Furnace and Resultant Products. US Patent Appl. 2005/0062205A1 (2005).

20. W.M. Goldberger, P.R. Carney, A.K. Reed. Thermal purification of natural mineral carbons. European Patent Appl. 87300021 (1987).

21. H. Ishizuka and Y. Sugano. Electrothermal fluidized bed furnace. US Patent Appl. US4158695 (1977).

22. J. Tuot. The electrothermal fluidized bed and its application to the production of titanium carbide. PhD Thesis, Department of Chemical Engineering of McGi11 University Montreal. Canada, August, 568 p. (1976).

23. M.V. Gubynskyi, I.V. Barsukov, S.S. Fedorov, M.V. Livitan, O.G. Gogotsi, U.S. Rohatgi. Study of Aerodynamic Properties of Continuous High Temperature Reactors. Proc. of ASME 2013 Fluids Engineering Div., Incline Village, NV (ASME FEDSM2013-16630) / Publ. BNL-99755-2013-CP - Nonproliferation and National Security Department, Brookhaven National Laboratory, U.S. Department of Energy, Office of Science NA242 (2013).

24. M.V. Gubynskyi, S.S. Fedorov, M.V. Livitan, R.G.Kheifetz and O.G. Gogotsi. Selection of aerodynamic modes for high-temperature electrothermal fluidized bed furnaces. Metallurhycheskaya teplotehnyka. Publ. of the National Metallurgical Academy of Ukraine, Dniepropetrovsk, Ukraine, 4(19)55-61 (2012) – in Russian.

25. A. Kozlov, Y. Chudnovsky, M. Khinkis, H. Yuan, M. Zak, and H. Yuan. Advanced Green Petroleum

Coke Calcination In Electrothermal Fluidized Bed. Book of Abstracts of 143th Annual Meeting & Exhibition; TMS Foundation, 2/16-20, 2014, San Diego, CA, USA (2014).

26. Y. Reynier, R. Yazami, B. Fultz, and I. Barsukov. Evolution of lithiation thermodynamics with the graphitization of carbons. J. Power Sources. 165 P. 552-558 (2007).

27. S.S. Fedorov. The analysis of the efficiency of high temperature segmental secondary heat utilizers of fluidized bed type. Part I. Metallurgical and Mining Industry. Dniepropetrovsk, Ukraine, 3, 125-128 (2013) – in Ukrainian.

28. S.S. Fedorov. The analysis of the efficiency of high temperature segmental secondary heat utilizers of fluidized bed type. Part II. Metallurgical and Mining Industry. Dniepropetrovsk, Ukraine, 4, 107-109 (2013) – in Ukrainian. .

29. V.S. Ostrovskiy, Yu.S. Virgiliev, B.I. Kostikov, et al. Synthetic graphite. Metallurgija Plubl. House, Moscow, USSR, 272 (1986) – in Russian.

30. I.G. Chernish, I.I. Karpov, G.P. Prikhodko, V.M. Shai, Physicochemical Properties of Graphite and Its Compounds, Naukova Dumka, Kiev, Ukraine, 198 (1990) - in Russian.

31. A.S. Fialkov. Carbon: The interlayer Compounds and Composite Materials Thereof. Aspect Press, Moscow, Russia, 718 (1997) – in Russian.

32. A.N. Kulik, A.N. Bugai, Y.V. Rogulskiy, O.B. Lysenko. Determination of the Specific Electric Resistance of Graphite at the high temperature using complex atomic absorption measurements. Journal of nano- and electronic physics. Web: 10 Feb. 2014<ssuir.sumdu.edu.ua/handle/123456789/1233>.

33. P. Kozhan, K. E. Makhorin, S. P. Gorislavets Electrical resistance of a fluidized bed of graphite particles. Journal of Engineering Physics and Thermophysics. 15 (4), 959-961 (1968) – in Russian.34. D. Kunii and O. Levenspiel. Ind. Eng. Chem. Process Design Developments. 7, 481 (1968).

35. O.M. Todesand O.B. Tsitovich. Fluidized bed reactors. Khimiya Publ. House, Leningrad, USSR. 296 (1981) – in Russian.

36. A. I. Malinovskiy, O.S. Rabinovich, V.A. Borodulya, A.Zh. Grebenkov, and A.M. Sidorovich. Local conductivity of fluidized bed filled with electrically conductive particles. Journal of Engineering Physics. 85 (2), 239 – 245 (2012) – in Russian.

37. G.N. Dulniev and V.V. Novikov. The processes of transfer in non-uniform environments. Energoatomizdat Publ. House, Leningrad, Russia, 248 (1991) – in Russian.

38. V.I. Lakomskiy. Electrical and electrocontact properties of electrode thermo-anthracite coal. Akademperiodika Publ. House, Kiev, Ukraine 106 (2008) - in Russian.

39. Grades of graphite and specifications: Product GT-1. Zavalyevskiy Graphite Ltd., Kyiv, Ukraine (2012).

40. State Standard Analytical Technique GOST 46684-75: Carbonaceous Materials. Harmonized Method for Measuring the Specific Electric Resistance of a Powder. GosStandart SSSR Publ. House, Moscow, USSR, 13 (1975) – in Russian.

41. Standard Test Method for Ash in a Graphite Sample: ASTM C561 - 91 (2010) e1. ASTM International, Book of Standards, Vol. 05.05, Subcom. D02.F0, P 2 (2010).